Analysis of Acoustic-Fields generated by Supersonic Jet Impinging on an Inclined Flat Plate and a Curved Plate

*Yuki Nagata[1], Taku Nonomura[2], Kozo Fujii[3], Makoto Yamamoto[4]

[1] Graduate School of Engineering, Tokyo University of Science, Japan
[2] Assistant professor, Japan Aerospace Exploration Agency, Japan
[3] Professor, Japan Aerospace Exploration Agency, Japan
[4] Professor, Tokyo University of Science, Japan

*Corresponding author: j4513639@ed.tus.ac.jp

Abstract

Flow and acoustic-fields of a supersonic jets impinging on an inclined flat plate and an inclined arc plate are computationally analyzed toward the prediction of the rocket plume acoustic waves. Effects to acoustic-field by changing plate angle and curvature of arc plate are investigated. A weighted compact nonlinear scheme is employed to solve 3-dimentional compressible Navier-Stokes equations. The results show that two acoustic waves generated near the jet impinging point affect the magnitude of sound pressure level near the fairing of the rocket and over-all sound pressure level becomes larger when curvature of arc plate increases.

Keywords: Mach wave, Interference wave, Shock wave, Separation bubble

Introduction

When launching a rocket, strong acoustic waves are generated from a jet plume impinging on the rocket launch site and they have bad influence on the satellite in the rocket. The report NASA-SP8072[1], proposed by NASA in 1971, is used for predicting acoustic waves over the world. However, it is based on the empirical model and its accuracy is not good enough for especially a new rocket launch site. It is necessary to understand the generation mechanism of acoustic waves for further improvements of the prediction model. Recently, analysis of acoustic waves of a rocket plume by using CFD has been conducted energetically at JEDI/JAXA, but it is limited to the practical one that simulates a real launch site for the support of the project in JAXA. Thus, fundamental knowledge has not been obtained. On the other hand, Nonomura et al[2]. and, Honda et al[3]. performed analyses of acoustic waves from a supersonic jet impinging on inclined flat plate. As a result, they classified variety of acoustic wave and obtained knowledge of a sound source for each acoustic wave. Main acoustic waves which have strong directivity are Mach waves generated from
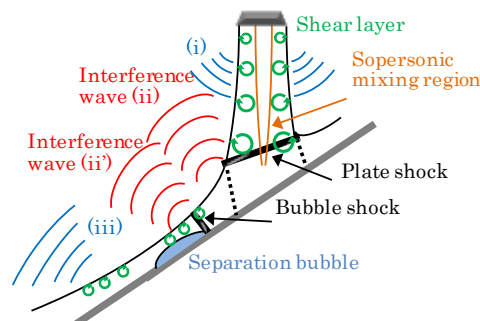
Figure 1. Schematic of jet flow and acoustic wave

sheer layers of supersonic region (Figure.1 (i),(iii)) and an interference wave generated by interference of turbulence and a shock wave generated at the region where the supersonic jet impinges on the wall or flow separates from the wall (Figure.1 (ii),(ii')). However, influence on the rocket by these acoustic waves have not been discussed. The purpose of this paper is, therefore, to understand the flow and acoustic fields for the prediction of acoustic waves. Moreover, we analyze

the influences of flat plate angle and plate curvature on flow and acoustic fields by conducting the computations with different value of those parameters.

Program settings

In the present study, air (specific heat ratio γ of 1.4) is used as fluid and an ideally-expanded jet is assumed. Thus, flowing three conditions; the ideally expanded Mach number M_j, the Reynolds number Re, and the temperature ratio TR_c. These parameters are related to the jet chamber condition and the ambient conditions by the assumption of isentropic expansion for the chamber to the nozzle exit.

$$M_J = \frac{u_J}{a_J} = \sqrt{\frac{2}{\gamma-1}\left\{\left(\frac{p_c}{p_\infty}\right)^{\frac{\gamma-1}{\gamma}}-1\right\}} \tag{1}$$

$$\mathrm{Re} = \frac{\rho_J u_J D}{\mu_\infty} \tag{2}$$

$$TR_C = \frac{T_c}{T_\infty} \tag{3}$$

where u, a, p, ρ and T denote the x-direction velocity, the speed of sound, the pressure, the density, and the temperature, respectively. Subscriptions J, c, and ∞ denote the nozzle exit condition (which is equivalent to the ideally expanded condition in this study), the chamber condition, and the ambient condition, respectively. M_j and Re are set to 2.0 and 100.000, respectively. Both Mach and Reynolds numbers are set to be lower values than those of rocket plumes, but high enough for the qualitative discussion for acoustic waves from rocket plumes.[4]

Figure.2 shows the jet profile used in this study. This profile consists of two parts, a center flat part and a boundary part which simulates the turbulent boundary layer with $(1/7)^5$ power low. Here, 99% thickness is 0.05D and the momentum thickness is approximately 0.006D.

Definitions of geometric parameters and the coordinate system are shown in Figure 2. In this study, flat plate angles θ are set to be 25 deg. to 70 deg. every 5 deg.. Here, TR_c is set to be 1.0. From previous work, we set the parameters to clearly observe an interference wave (ii).
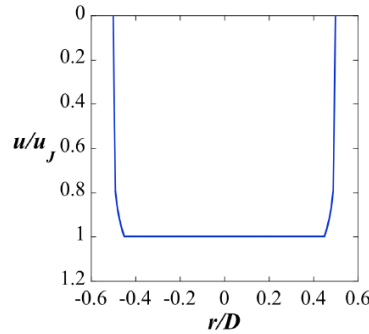
Figure 2. JET-plofile

The Strouhal number and the sound pressure level(SPL) are defined as follows.

$$St = \frac{fD_j}{u_j} \tag{4}$$

$$SPL[dB] = 20\log_{10}\frac{\tilde{p}}{\tilde{p}_{ref}} \tag{5}$$

where f is frequency, $\tilde{p}$ is effective pressure fluctuation and $\tilde{p}_{ref}$ is the reference SPL in our computation which is defined as follows.

$$\tilde{p}_{ref} = \frac{2 \times 10^{-5}[pa]}{101300[Pa]} \times p_{\infty} \tag{6}$$

In this study, computational cases are plate angle θ=25 deg. to 70 deg.(every 5 deg.) and L/D is 5.0 for the case with an inclined flat plate, $5D$ radius and L/D is approximately $7.5D$ for the case with curved plate. Figure.3 shows schematic of flat and curved plates.
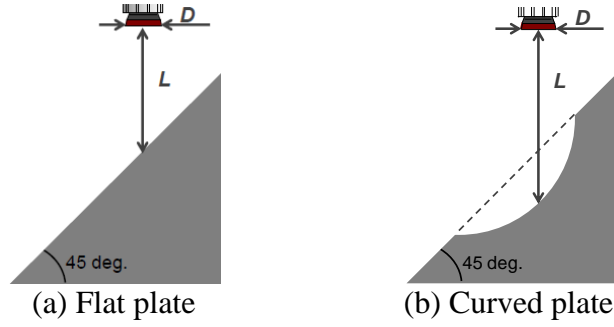

(a) Flat plate   (b) Curved plate
Figure 3. Schematic of launch site

Computational approach
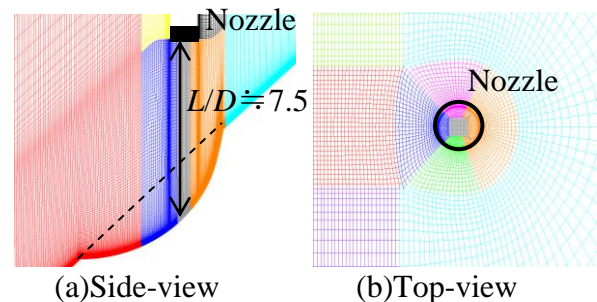
Computational grids

Figure 4 shows computational domain. Orange area is computational domain, and the outside, buffer region[6](sky blue region in Fig.4) stretched to prevent acoustic wave from nonphysical reflecting and generating is set up. Stretching ratio of grid is 1.03 on a boundary of computational domain, and raised the ratio gradually to 1.2 as far from computational domain.Figures.5 and 6 show computational grids. In this study, it is important how to resolve downstream flow after impinging. Therefore, fine grids are required for those regions. In this study, entire computational domain is divided into 11 zones, and physical quantities are interpolated between each grids. However, grid points are over-lapped by 16 points, thus, no error due to interpolation are produced. A number of grid points is 150 on the center line of nozzle (*x*-direction), 106 in the direction apart from the axis(upstream-direction), 206(downstream-direction), and 197 in the direction around circumference. Total grid points are approximately 8 million.
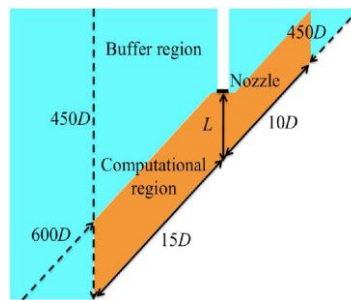
Figure 4. Computational domain
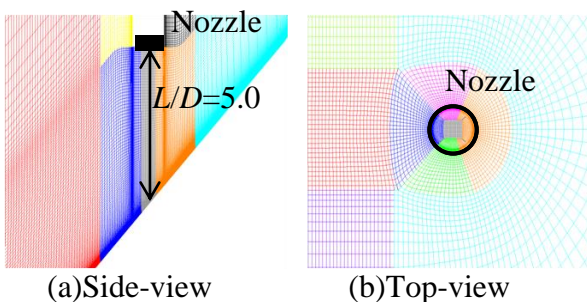
(a)Side-view   (b)Top-view   (a)Side-view   (b)Top-view
Figure 5. Computational grids(Flat plate)   **Figure 6. Computational grids(Arc plate)**

3

Computational scheme

Government equation is three-dimension compressible Navier-Stokes equation non-dimensionalized by diameter of the nozzle, the ambient density, and the ambient sound speed[7]. Seventh order weighted compact nonlinear scheme (WCNS) and sixth order central difference are used for discretization of convective and viscous terms, respectively. Here, WCNS was developed by Deng[8] as mixture of weighted essentially non-oscillatory (WENO) scheme [9] and compact difference scheme.[10] Although the original WCNS is 5th order, recently it is extended to 9th order by Nonomura et al[11], Zhang et al[12], independently. The resolution of WCNS is higher than WENO method in terms of resolution. Besides, WCNS method have merits that it can hold freestream.[13] Simple high resolution upwind scheme[14] is used to evaluate flux in WCNS method. In this study, below devise is used to raise computational velocity. When seeking physical quantity $\tilde{U}_{j+1/2}^{L}$ at cell boundary, computing is conducted as follows:

$$\tilde{U}_{j:k}^{(n)} = \left(\frac{1}{\Delta x}\right)^{n} \sum_{l=0}^{r-1} a_{k:l}^{n} U_{j-r+k+l} \tag{7}$$

$$\tilde{U}_{j+1/2:k}^{L} = U_{j} + \sum_{n=1}^{r-1} \left(\frac{\Delta x}{2}\right)^{n} \left(\frac{1}{n!}\right) \tilde{U}_{k:l}^{(n)} \tag{8}$$

$$IS_{j:k} = \sum_{n=1}^{r-1} \left(\tilde{U}_{j:k}^{(n)}\right)^{2} \cdot \quad IS_{j:k} = \begin{cases} IS_{j:k} & \dfrac{\max(IS_{j:l})}{\min(IS_{j:l})} > R \\ \\ 0 & \dfrac{\max(IS_{j:l})}{\min(IS_{j:l})} < R \end{cases} \tag{9}$$

$$\alpha_{k} = \frac{C_{k}}{(IS_{k} + \varepsilon)^{p}} \tag{10}$$

$$w_{k} = \frac{\alpha_{k}}{\sum_{i=1}^{r} \alpha_{i}} \tag{11}$$

$$\tilde{U}_{j+1/2}^{L} = \sum_{k=1}^{r} w_{k} \tilde{U}_{j+1/2:k}^{L} \tag{12}$$

Here, w_{k} is a non-linear weight.

Monotonicity integrated large-eddy simulation is adopted[15] and that the numerical viscosity of upwind difference scheme is used for turbulence eddy viscosity as the subgrid scale model of LES. Therefore, any explicit subgrid scale models are not used. For the time integration, second order backward difference scheme is converged using an implicit method and inner iterations. For an implicit method, alternative directional implicit symmetric Gauss-Seidel scheme[17] which adopt the upwinding by the spectral radius to each direction of lower-upper alternative directional implicit scheme[16] is used. Three inner iterations employed. Time step is set so that the maximum CFL number is approximately 10 (near the shock wave and shear layer, less than 1), the non-dimensional integration time is 400, and the minimum resolved Strouhal number is approximately 0.02(cold jet),0.007(hot jet) considering the sound pressure oscillation is included more than 10 periods in integration times. Regarding the boundary condition, static pressure is set to be the ambient condition at the exit boundary and no-slip condition is used at the wall surface. For evaluation of the sound pressure, the pressure fluctuation is analyzed as the sound pressure in the computational domain. On the other hand, in the far field, after fast Fourier transform of the integral surface, the Kirchhoff method[18] is used to predict the sound pressure in frequency domain. An integral surface is set to be the outside of the computational domain, and this domain is enough far to pick up no pressure fluctuation due to the flow motion (pseudo sound wave) in near field. However, the sound pressure level of acoustic waves generated in the present computation is very high, and it seems that non-linearity seems to be included in acoustic wave propagation. Since the Kirchhoff method does not allow non-linear propagation of acoustic waves, it seems that the correct sound pressure level

distribution is not obtained quantitatively. However, it does not matter for the objective of the present study: the qualitative reorganization of mechanism of acoustic wave generation.

Results and discussion

Effect of changing angle of inclined flat plate

Figure7 shows sound pressure level distribution for the cases with different plate angles. It shows that Mach waves (i) generated from the sheer layer before impinging, interference waves (ii) are generated by interference of the sheer layer and the shock wave. Moreover, when the plate angle exceed 45 deg., acoustic wave (ii') generated by the bubble shock is observed.

(a) 25 deg.   (b) 40 deg   (c) 55 deg.   (d) 70 deg.

140   180 [dB]
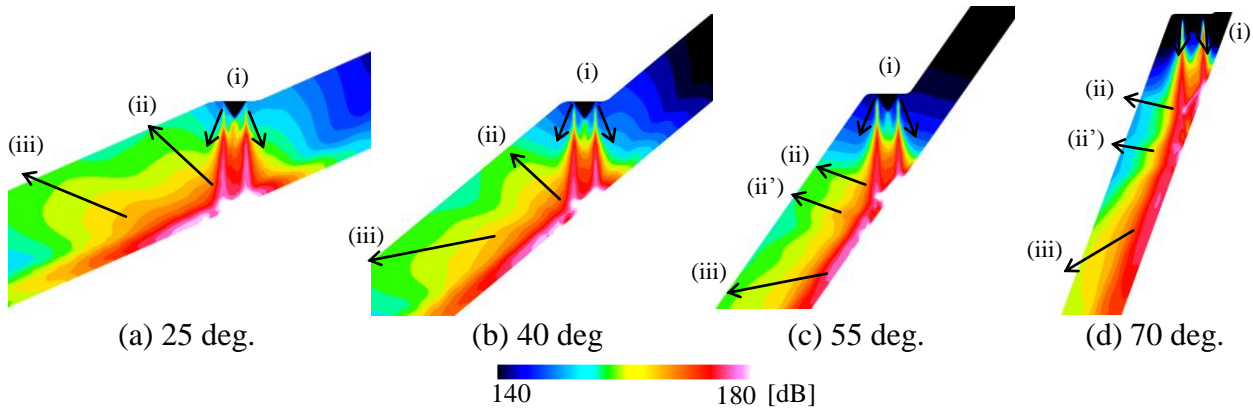
Figure 7. OASPL Distribution of Symmetry plane

The location of source of interference wave (ii) overlaps with that of (ii') in near field, As a result, these two acoustic waves seem to behave as one kind of acoustic waves in far field. Since it may have main influence on a rocket, it is focused on in this study. Figure 8 shows peak OASPL(Over all Sound Pressure Level) of this kind of acoustic waves at 20D from the point of jet impinging. The horizontal axis shows the plate angle, θ. It shows that OASPL has the local maximum at 50 deg.. Since interference wave (ii) is weaker as the plate angle rises[19],interference wave (ii) is dominant at 40 deg., on the other hand, interference wave (ii') is dominant from 45 deg. to 50 deg.. Figure.9 shows OASPL at 20D vertically from the point of jet impinging (this point is located at the rocket fairing). It can be seen that OASPL decreases as θ increases. Moreover. when θ is over 50 deg., OASPL decreases sharply. It seems that the superposition of interference wave (ii) and (ii') has the significant effects on the sound pressure at the rocket fairing because OASPL of superposition of interference wave (ii) and (ii') is also decreased sharply over 50 deg.. However, further investigation is necessary to conclude this.
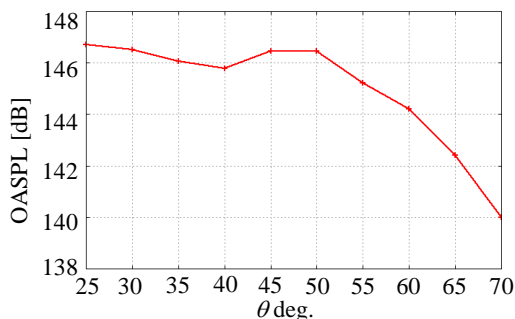

Figure 8. Superposition of interference wave (ii),(ii') at 20D
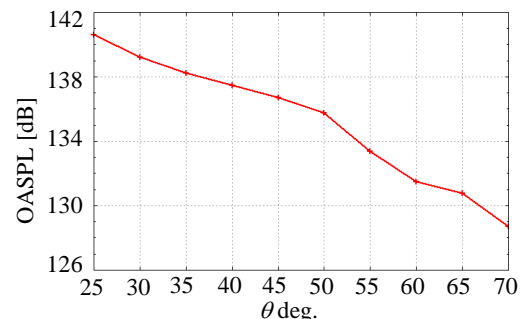
Figure 9. OASPL at the rocket fairing

Figure 10 shows three quantities for the cases with flat plate. Firstly, the vertical axis at left side shows the peak OASPL of interference wave (ii') at 1.5D from the wall surface. The vertical axis at

5

the right side shows the others, strength of the bubble shock (pressure ratio before and after bubble shock) and thickness of separation bubble. It can be seen that strength of the bubble shock and thickness of a separation bubble have similar trend and become the maximum at 55 deg., together (this is same in all angles less than 50 deg.). Therefore, it seems that the thicker separation bubble makes bubble shock stronger. Since the stronger shock wave makes the acoustic waves caused by the shock stronger, the strength of bubble shock seems to be correlated with the interference wave (ii'). However, OASPL of the interference wave (ii') becomes maximum at 50 deg.. At 50 deg., it may be that the interference wave (ii) influenced on the interference wave (ii') because the position of occurrence of interference wave (ii') is nearer to interference wave (ii) than the other angles in the horizontal axis of Fig.10.
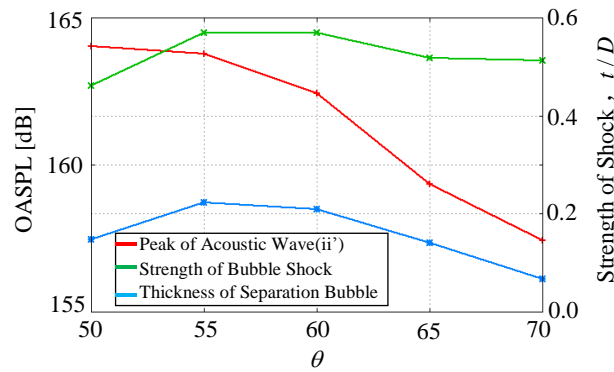

**Figure 10. Relation of Acoustic Wave(ii') and Flow Factor**

Effect of launch site's curvature

Effect of curvature of launch site is discussed by comparing the case with a curved plate with the case with a flat plate. The cases with 45 deg. inclined flat plate and curved plate of curvature of 5*D* (angle of flat plate part is 45 deg.) are considered, respectively. Distance from the nozzle exit to the impinging point is 5.0*D* for the case with the flat plate, approximately 7.5*D* for the case with the curved plate. Figure 11 shows that SPL distribution at near field of the case with curved plate. It can be seen that acoustic waves are generated similar to the case with the flat plate.

Here, OASPL of flat plate at the rocket fairing is 134.7 dB, on the other hand, that of curved plate is 135 dB. Goto et al.[20] confirmed that OASPL of acoustic wave decreases as *L/D* becomes larger for flat plate cases. Though the case with the curved plate has larger *L/D* (approximately 7.5) than the case with the flat plate (5.0), OASPL of curved plate at the rocket fairing is larger. Figure 13 shows these two cases of OASPL on arc of radius 20*D*, 50D, 100*D*, around impinging point (see Figure 12, though it is not exactly scaled). The horizontal axis α is the angle measured from the wall in a downstream side. It shows that a rise in OASPL due to interference wave (ii), (ii'), and
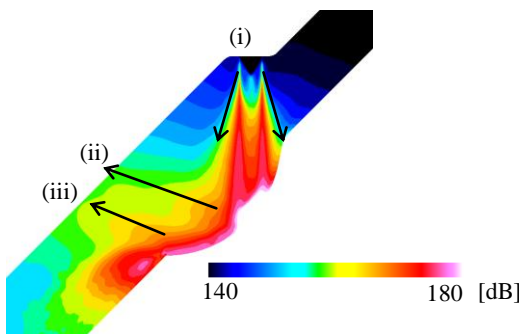

Figure 11. OASPL distribution of symmetry plane
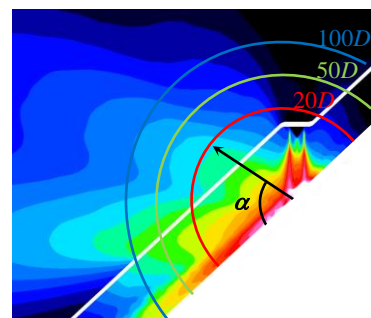
**Figure 12. Measurement position of SPL**

Mach wave (iii).both cases. In the case with a curved plate, one OASPL peak can be observed,

6

although they are two peaks in flat plate case. It is thought that the Mach wave (iii) overlapped with interference wave (ii) and (ii') because the Mach wave (iii) propagates upward by a curvature of wall surface.
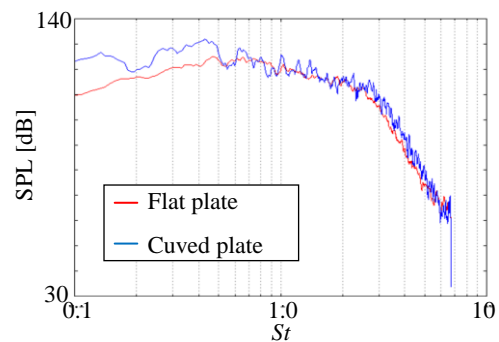

(a) Flat plate

(b) Curved plate
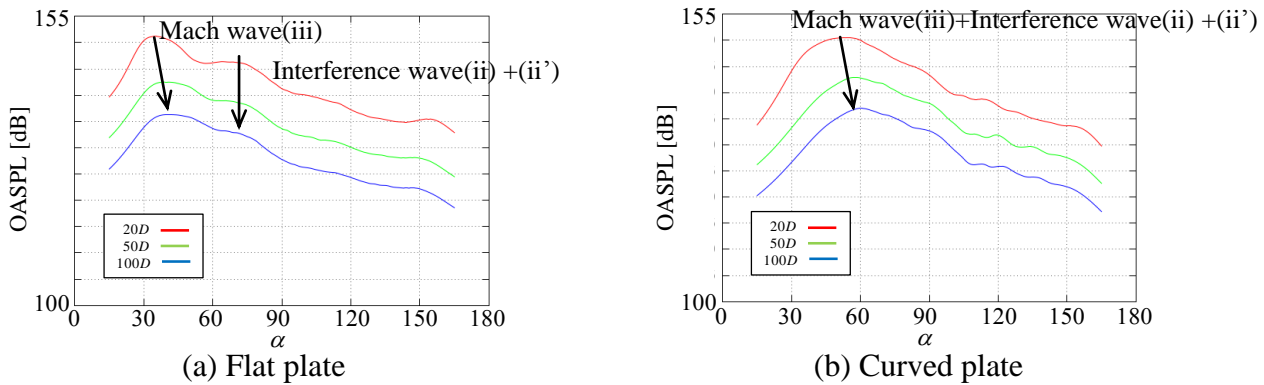
**Figure 13. Far field directivity**

Figure 15 shows the spectra of SPL at the points defined in Figure 14. Points A, B, and C are located at the position for Mach wave(iii), superposition of interference wave(ii) and (ii'), and rocket faring, respectively. At the point A, α is 32.5 deg. for the flat plate. At the point B, α is 61 deg. for the flat plate, 52.5 deg. for the curved plate. At the point C, α is 135 deg. It can be seen that the case with a curved plate has lower peak in the Strouhal number of the spectrum than the case with a flat plate in terms of Strouhal number of the spectrum peak from Figure 15. Figure 16 shows spectra of the Mach wave (iii) and superposition of the interference wave (ii) and (ii') at 20D from the impinging point for the case with flat plate of 45 deg.. It can be seen that the frequency of the Mach wave is generally lower than that of the interference wave. Moreover, also it can be seen that the peak of spectrum of acoustic waves in the case of the curved plate is lower than that of the case with the flat plate in terms from Figure 17. Therefore, it may be that Mach wave(iii) has influence on the sound pressure level at the rocket fairing in the case with the curved plate.
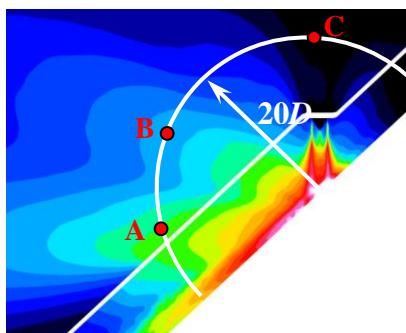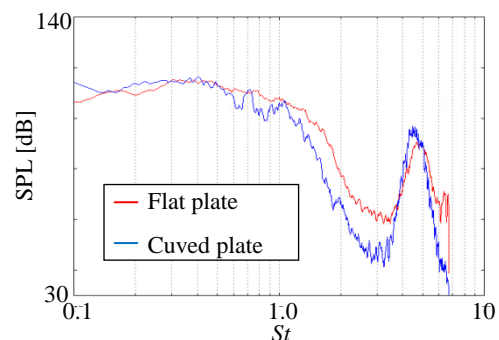

Figure 14. Measurement point of spectra of SPL

Figure 15. Spectra of SPL at pointB
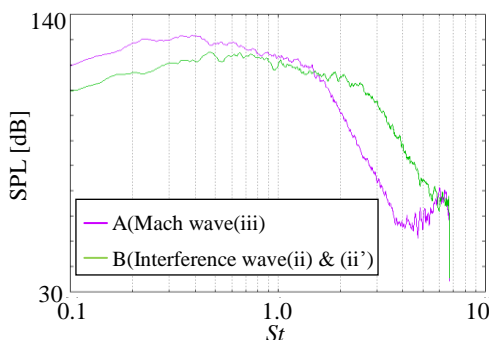
Figure 16. Spectra of SPL at pointA, B

Figure 17. Spectra of SPL at pointC(rocket fairing)

7

Conclusion

Analysis for flow and acoustic fields of a supersonic jet impinging on an inclined flat plate and a curved plate was conducted and, as a result, following knowledge was obtained.

(a) Interference waves (ii) overlaps with (ii') in near field, as a result, they behaves as one kind of acoustic waves in far field, and OASPL of this kind of acoustic waves are according to magnitude of interference wave(ii) and (ii').
(b) Sound pressure level of superposition of the interference waves (ii) and (ii') is sharply changed when the plate angle becomes more than 50 deg..
(c) Making the plate angle more than 50 degrees significantly reduces OASPL at the rocket fairing.
(d) A launch site with no curvature prevents the Mach waves (iii) propagating into the rocket fairing.

References

(1) Eldred, S. (1971) "Acoustic Loads Generated by Propulsion System," NASA SP-8072(1971).
(2) Nonomura ,T. , Goto ,Y. , Fujii ,K. "Acoustic Waves from a Supersonic Jet Impinging on an Inclined Flat Plate," AIAA paper 2011-476(2010)
(3) Honda ,H. , Nonomura ,T. , Fujii ,K. , Yamamoto ,M. "Effects of Plate Angles on Acoustic Waves from a Supersonic Jet Impinging on an Inclined Flat Plate," AIAA paper 2011-3260(2011).
(4) Nonomura, T.,Characteristics of Acoustic Waves Generated by Flow Instability of Supersonic Jets, Ph.D. thesis, University of Tokyo, 2008.
(5) Pope, S. B.,Turbulent Flows, Cambridge University Press, 2000
(6) Borre, S., Bogey, C. and Baily, C. (2006), "Computation of the Noise Radiated by Jets with Laminar/Turbulent nozzle-exit conditions," AIAA-paper 2006-2443.
(7) T, Colonius, S. K. Lele and P. Moin, "Boundary Condition for Direct Computation of Aerodynamics Sound Generation," AIAA Journal, vol. 31, No. 9(1993).
(8) Fujii ,K., "Numerical Methods for Computational Fluid Dynamics (1994).
(9) Deng, X. G. and Zhang, H., "Developing high-order weighted compact nonlinear schemes," Journal of Computational Physics, 165(2000), pp.22-44.
(10) Jiang, G.-S. and Shu, C.-W., "Efficient implementation of weighted ENO schemes", J. Comput. Phys，126, (1996), pp. 200-212.
(11) Lele, S. K., "Compact Finite Difference Schemes with Spectral-Like Resolution," Journal of Computational Physics, 103(1992), pp. 16-42.
(12) Nonomura, T., Iizuka, N. and Fujii, K., 2007, "Increasing Order of Accuracy of Weighted Compact Non-Linear Scheme." AIAA Paper 2007-0468(2007).
(13) Zhang, S., Jiang, S. and Shu, CW., "Development of nonlinear weighted compact scheme with increasingly higher order accuracy," Journal of Computational Physics, 227(2008), pp. 7294-7321.
(14) Nonomura, T., Iizuka, N. and Fujii, K., "Uniform preserving property of higher order upwind finite difference scheme on generalized coordinate system," Proceedings of 4th International Conference of Computational Fluid Dynamics.(2006).
(15) Boris, J. P., Grinstein, F. F., Oran, E.S. and Kolbe, R. J., 1992, "New Insights Into Large Eddy Simulation," Fluid Dynamics Research, Vol. 10, pp. 199-288.
(16) Fujii, K. and Obayashi, S., "Practical Applications of New LU-ADI Scheme for the Three-Dimensional Navier-Stokes Computation of Transonic Viscous FLows" AIAA paper 86-0513(1986).
(17) Fujii, K, "The frontier of finite volume method-Recent trend of High-speed air flow numerical methods"，JSCES journal，Volume 3, Item 3 pp. 158-166
(18) Pan, F.L., Uzun, A. and Lyrintzis, A. S., "Refraction Corrections for Surface Integral Methods in Jet Aeroacoustics," AIAA paper 2004-2873(2004).
(19) Ted,A.,Manning, "A NUMERICAL INVESTIGATION OF SOUND GENERATION IN SUPERSONIC JET SCREECH " (1999)
(20) Goto ,Y. , Nonomura ,T. , Fujii ,K. , "Relation between Jet Potential Core Length and Nozzle-Plate Distance for Acoustic Waves from a Supersonic Jet Impinging on an Inclined Flat Plate," JSASS paper U-7(2009).